Analysis and Multi-Objective Optimal Design of a Planar Differentially Driven Cable Parallel Robot

Ruobing Wang† and Yangmin Li†*

†*Department of Industrial and Systems Engineering, The Hong Kong Polytechnic University, Kowloon, Hong Kong SAR, China*

SUMMARY
In this work, a planar cable parallel robot (CPR) driven by four cables and pulley differentials is proposed and analyzed. A new cable and pulley differential is designed by adding an extra pulley to eliminate the modeling inaccuracies due to the pulley radius and obviate the need of solving the complex model which considers the pulley kinematics. The design parameters of the proposed CPR are determined through the multi-objective optimal design for the largest total orientation wrench closure workspace (TOWCW) and the highest global stiffness magnitude index (GSMI). The proposed differentially driven CPR is evaluated by comparing various performance indices with a fully actuated CPR.

KEYWORDS: Cable parallel robot; Cable and pulley differential; Kinematics; Statics; Multi-objective optimal design.

1. Introduction
Cable parallel robots (CPRs) are a particular kind of parallel robots which their moving platforms (MPs) are connected to the bases through exible cables. CPRs have some potential merits include low mass and inertia, highly dynamic response, large workspace, large load to weight ratio, effective use of materials, and efficient power transmission. While the main drawbacks of CPRs are high exibility and relative low positioning accuracy.[?] CPRs have been widely used in cable-suspended camera systems, construction cranes, large radio-telescopes, haptic devices, rehabilitation robotics, and material handling applications. [?,?]

CPRs can be considered as under-constrained or fully constrained according to the number of actuated cables. CPRs with n degrees of freedom (DOFs) are under-constrained if they are driven by $m \leq n$ cables. The under-constrained CPRs have a lower cost since fewer actuators are used and have a lower risk of collision due to the fewer numbers of cables. [?] However, they have drawbacks in accuracy and stiffness and are hard to be controlled. The fully constrained CPRs are actuated by $m > n$ cables. The fully constrained CPRs have some merits such as higher stiffness and a larger workspace. [?]While the problems of cost, collision, and control complexity will become more critical with the number of cables increases. Therefore, it's a dilemma to increase the number of actuated cables to improve performance and to reduce the cost and complexity of CPRs.

One of the solutions to this predicament is to use cable differentials to increase the number of actuated cables while without changing the number of actuators. Khakpour et al. first introduce the cable differentials into the design of 2-DOF planar CPRs and propose the possible arrangements for cable differentials with a different number of cables. [?] Then the workspace augmentation using cable differentials is investigated for 3-

* Corresponding author. E-mail: yangmin.li@polyu.edu.hk

DOF spatial cases.[?,?] The stiffness of 2-DOF planar differentially driven CPRs is analyzed in ref. [?] and the authors show that it's a conflict to improve the workspace and stiffness simultaneously. Similar works using cable differentials to actuate CPRs also include refs. [?,?].

However, in most previous works using cable differentials, only single-point MPs are adopted and the effects of using cable differentials on orientation workspace are never investigated. Besides, most of the differentially driven CPRs in previous works are designed by intuition, a systematic design approach is needed to make the differentially driven CPRs achieve the best performance. Furthermore, except for workspace and stiffness, other performance indices like dexterity and manipulability are not verified for the CPRs using cable differentials. Moreover, in previous works, the kinematics of cable differentials are generally simplified to the point-to-point model, and the pulley radius is neglected, which introduces inherent modeling errors to the robot kinematics.

Many recent works have been addressed for the design and analysis of CPRs. In ref. [?], a two-phase geometry selection strategy is proposed for geometry selection of a redundant CPR. The first phase of proposed method is to test a very large number of possible cable arrangements using a novel performance index. The positions of cable drawing points are refined in the second phase. In ref. [?], the wrench exertion capability is used to evaluate the performances of planar and spatial CPRs. This index represents the maximum wrench that cables can exert on the MP along a certain direction over the workspace. In ref.[?], the force transmission indices are used to optimize the geometric parameters of a 3-DOF translational CPR. The orthogonal-degree-based local actuation index and local constraint index are defined and compared with the manipulability index. In ref. [?], a combined methodology is proposed for type and size optimization of CPRs used for upper-limb rehabilitation exercises. The objective of the proposed method is to minimize the occupied volume by the robot and minimize the cable tensions. The above works provide great inspirations for the design and analysis of CPRs. However, these works all focus on fully actuated CPRs which have the same number of cables and actuators. So the methods and results in these works cannot be directly applied to differentially driven CPRs.

In this work, the effects of cable and pulley differentials are investigated on the design of a 3-DOF planar CPR. Inspired by the works in refs. [?,?], a new cable and pulley differential is designed by adding an extra pulley to eliminate the modeling inaccuracies due to the pulley radius and obviate the need of solving the complex model which considers the pulley kinematics. The geometry of the proposed CPR is determined through the multi-objective optimal design for the largest workspace and the highest stiffness magnitude using the genetic algorithm. The multi-objective optimal design adopted in this paper gives more potential useful solutions compared with the commonly adopted optimal design approaches in parallel robots which convert the multiple objectives to a single function. In the end, various performance indices are used to evaluate the proposed robot by comparing with a fully actuated CPR to show the effects of using cable and pulley differentials in all aspects.

The main contributions of this work include the following. (1) A novel cable and pulley differential is designed by adding an extra pulley to simplify the kinematic and static equations. (2) A 3-DOF planar differentially driven CPR is firstly proposed by adopting the novel cable and pulley differentials. (3) A multi-objective optimization approach is proposed to determine the structural parameters of the proposed CPR. (4) The performance of the proposed differentially driven CPR is evaluated by a thorough comparison with a fully actuated CPR using various performance indices.

The remaining parts of this paper are arranged as follows. Section **??** describes the kinematics and statics equations of the cable and pulley differential. Section **??** gives the kinematics and statics analysis of the proposed differentially driven CPR. Section **??** lists the performance indices used in this paper and the multi-objective optimal design of the proposed robot is conducted in Section **??**. Section **??** gives the comparison of the

proposed differentially driven CPR with the fully actuated CPR and Section **??** gives the conclusions.

2. Kinematics and Statics of the Cable and Pulley Differential

2.1. Cable and Pulley Differential

The cable differential is a mechanism that couples and transmits the output of a single actuator to several cables. It can be used on CPRs to increase the number of actuated cables without changing the number of actuators. In this work, we focus on the 2-cable differential using the cable and pulley system due to its simple structure.

Fig. **??** shows the schematic of the i-th cable and pulley differential on the CPR. The red lines represent cables and the blue lines represent forces applied by cables. The cable which exits from the winch goes through two pulleys located at points A_{i1} and B_i respectively, and finally is attached to point A_{i2}. Points A_{i1} and A_{i2} locate on the base and point B_i is on the MP of the robot. Assuming the coordinates of these points in the base frame are $A_{i1} = [a_{i1x}\, a_{i1y}]^T$, $A_{i2} = [a_{i2x}\, a_{i2y}]^T$ and $B_i = [b_{ix}\, b_{iy}]^T$. To control the CPR, the cable length of the cable and pulley differential needs to be solved according to the position of MP. The total cable length l_i of the i-th cable and pulley differential can be determined by summing up the following parts

$$l_i = l_{i0} + l_{i1} + l_{i2} + l_{Ai1} + l_{Bi}, \tag{1}$$

where l_{i0} is the constant cable length between the winch and the guiding pulleys, l_{i1} is the length of free cable between the pulleys at points A_{i1} and B_i, l_{i2} is the length of free cable between the pulleys at points A_{i2} and B_i, l_{Ai1} is the length of wrapping cable around the pulley at point A_{i1}, and l_{Bi} is the length of wrapping cable around the pulley at point B_i. Assuming that the pulleys at point A_{i1} and B_i have the same radius r_P, then l_{i1} can be determined directly by the distance between the two points as

$$l_{i1} = \sqrt{(a_{i1x} - b_{ix})^2 + (a_{i1y} - b_{iy})^2}. \tag{2}$$

l_{i2} cab be determined by the distance between points A_{i2} and B_i as

$$l_{i2} = \sqrt{(a_{i2x} - b_{ix})^2 + (a_{i2y} - b_{iy})^2 - r_P^2}. \tag{3}$$

The distance between points A_{i1} and A_{i2} is denoted as d_i, which can be calculated as

$$d_i = \sqrt{(a_{i1x} - a_{i2x})^2 + (a_{i1y} - a_{i2y})^2}. \tag{4}$$

Denote the wrapping angle around the pulleys at points A_{i1} and B_i as θ_{Ai1} and θ_{Bi} respectively. According to the law of cosines in trigonometry, we have

$$\theta_{Ai1} = \pi - \arccos\frac{l_{i1}^2 + d_i^2 - l_{i2}^2 - r_P^2}{2l_{i1}d_i}, \tag{5}$$

$$\theta_{Bi} = \frac{3}{2}\pi - \arccos\frac{l_{i1}^2 + l_{i2}^2 + r_P^2 - d_i^2}{2l_{i1}\sqrt{l_{i2}^2 + r_P^2}} - \arctan\frac{l_{i2}}{r_P}. \tag{6}$$

Then l_{Ai1} and l_{Bi} can be calculated as

$$l_{Ai1} = r_p\theta_{Ai1}, \tag{7}$$

$$l_{Bi} = r_P\theta_{Bi}. \tag{8}$$

Combining (**??**) to (**??**), l_i can be solved in closed-form as

$$
\begin{aligned}
l_i =\, & l_{i0} + \sqrt{(a_{i1x} - b_{ix})^2 + (a_{i1y} - b_{iy})^2} + \sqrt{(a_{i2x} - b_{ix})^2 + (a_{i2y} - b_{iy})^2 - r_P^2} + \\
& \left(\arcsin \frac{(a_{i1x} - a_{i2x})(a_{i1x} - b_{ix}) + (a_{i1y} - a_{i2y})(a_{i1y} - b_{iy})}{\sqrt{(a_{i1x} - a_{i2x})^2 + (a_{i1y} - a_{i2y})^2}\sqrt{(a_{i1x} - b_{ix})^2 + (a_{i1y} - b_{iy})^2}} + \right. \\
& \arcsin \frac{(a_{i1x} - b_{ix})(a_{i2x} - b_{iy}) + (a_{i1y} - b_{iy})(a_{i2y} - b_{iy})}{\sqrt{(a_{i1x} - b_{ix})^2 + (a_{i1y} - b_{iy})^2}\sqrt{(a_{i2x} - b_{ix})^2 + (a_{i2y} - b_{iy})^2}} - \\
& \left. \text{arccot} \frac{r_P}{\sqrt{(b_{ix} - a_{i2x})^2 + (b_{iy} - a_{i2y})^2 - r_P^2}} + \frac{3}{2}\pi \right) r_P.
\end{aligned}
\tag{9}
$$

To analyze the static stability of the CPR, the force applied by the cable and pulley differential on the MP needs to be solved. Denote the cable forces along cable segments l_{i1} and l_{i2} as $\boldsymbol{f}_{i1}$ and $\boldsymbol{f}_{i2}$ respectively. Assuming the pulley friction is ignorable, then all cable segments have the same tension denoted as t_i. The resultant force $\boldsymbol{f}_i$ applied by the i-th cable and pulley differential on the MP can be derived according to the following equations

$$
\boldsymbol{f}_{i1} = \frac{t_i}{l_{i1}} \begin{bmatrix} a_{i1x} - b_{ix} \\ a_{i1y} - b_{iy} \end{bmatrix},
\tag{10}
$$

$$
\boldsymbol{f}_{i2} = \frac{t_i}{l_{i2}} \begin{bmatrix} a_{i2x} - b_{ix} + r_P \sin(\theta_{Ai1} + \theta_{Bi}) \\ a_{i2y} - b_{iy} + r_P \cos(\theta_{Ai1} + \theta_{Bi}) \end{bmatrix},
\tag{11}
$$

$$
\boldsymbol{f}_i = \boldsymbol{f}_{i1} + \boldsymbol{f}_{i2}.
\tag{12}
$$

It can be seen from the above equations that the resultant force $\boldsymbol{f}_i$ generally has a larger magnitude than the cable forces $\boldsymbol{f}_{i1}$ and $\boldsymbol{f}_{i2}$ if the angle θ_{Bi} is not too small. Besides, the resultant force $\boldsymbol{f}_i$ lies on the bisector of the two cable segments l_{i1} and l_{i2} due to the equal magnitude of $\boldsymbol{f}_{i1}$ and $\boldsymbol{f}_{i2}$. Let point S_i be the intersection of the resultant force $\boldsymbol{f}_i$ and line $A_{i1}A_{i2}$. At this moment, the cable and pulley system can be considered as a single cable connecting points B_i and S_i with force $\boldsymbol{f}_i$. With the change of the MP position, point S_i moves between points A_{i1} and A_{i2}, which changes the position of virtual attachment point on the base. These properties of using cable differential are beneficial to the design of CPRs, which will be shown in later sections.

2.2. Novel Cable and Pulley Differential with Extra Pulley

Equations (**??**) and (**??**) give the kinematics and statics relations of the cable and pulley differential. However, considering these equations will increase the model complexity and bring difficulties to the design and control of differentially driven CPRs. Neglecting the pulley radius and considering the cables as point-to-point connections may be a reasonable choice in some situations but it will introduce inherent modeling errors. Thus a new cable and pulley differential is designed by adding an extra pulley to eliminate the modeling inaccuracies due to the pulley radius and obviate the need of solving the complex model which considers the pulley kinematics.

The new cable and pulley differential on the CPR is shown in Fig. **??**, a pulley with the radius r_P is attached to point A_{i2} on the base. The wrapping angle and wrapping cable length around the added pulley are denoted as θ_{Ai2} and $l_{Ai2} = r_P \theta_{Ai2}$, respectively. The added pulley at point A_{i2} alters the cable length l_{i2} as

$$
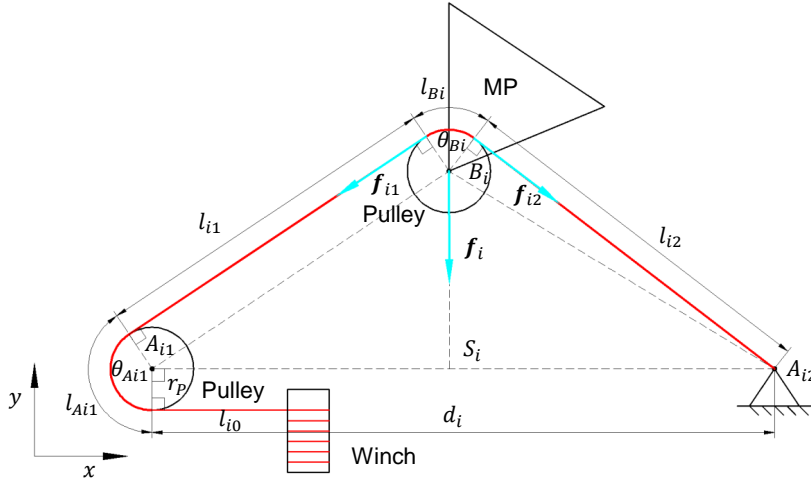l_{i2} = \sqrt{(a_{i2x} - b_{ix})^2 + (a_{i2y} - b_{iy})^2}.
\tag{13}
$$

Fig. 1. Schematic of the i-th cable and pulley differential on the CPR.

Since all the pulleys of the new cable and pulley differential have the same radius, we have

$$\theta_{Ai1} + \theta_{Ai2} + \theta_{Bi} = 2\pi. \tag{14}$$

Thus the total cable length l_i of the i-th new cable and pulley differential can be solved as

$$
\begin{aligned}
l_i =& l_{i0} + l_{i1} + l_{i2} + l_{Ai1} + l_{Ai2} + l_{Bi} \\
=& l_{i0} + 2\pi r_P + \sqrt{(a_{i1x} - b_{ix})^2 + (a_{i1y} - b_{iy})^2} + \sqrt{(a_{i2x} - b_{ix})^2 + (a_{i2y} - b_{iy})^2} \\
=& l'_{i0} + \sqrt{(a_{i1x} - b_{ix})^2 + (a_{i1y} - b_{iy})^2} + \sqrt{(a_{i2x} - b_{ix})^2 + (a_{i2y} - b_{iy})^2}.
\end{aligned}
\tag{15}
$$

where l'_{i0} is the length of cable segments that remain constant during the movement of the MP.

Through adding the extra pulley, the cable segments l_{i1} and l_{i2} become parallel to lines $A_{i1}B_i$ and $A_{i2}B_i$, respectively. Hence the resultant forces of $\boldsymbol{f}_{i1}$ and $\boldsymbol{f}_{i2}$ go along the direction of the bisector of lines $A_{i1}B_i$ and $A_{i2}B_i$. The resultant force $\boldsymbol{f}_i$ on the MP becomes

$$
\begin{aligned}
\boldsymbol{f}_i =& \boldsymbol{f}_{i1} + \boldsymbol{f}_{i2} \\
=& \frac{t_i}{l_{i1}} \begin{bmatrix} a_{i1x} - b_{ix} \\ a_{i1y} - b_{iy} \end{bmatrix} + \frac{t_i}{l_{i2}} \begin{bmatrix} a_{i2x} - b_{ix} \\ a_{i2y} - b_{iy} \end{bmatrix}.
\end{aligned}
\tag{16}
$$

Equations (**??**) and (**??**) indicate that the kinematics and statics equations of the new cable and pulley differential are consistent with the point-to-point model which neglects the pulley radius. Thus the radius of the pulley will not affect the kinematics and statics analysis of CPRs. The simplification of the kinematics and statics of the cable and pulley differential brings convenience to the design and analysis of differentially driven CPRs.

3. Kinematics and Statics of the Differentially Driven CPR

3.1. Kinematics Analysis
The proposed 3-DOF planar differentially driven CPR as shown in Fig. **??** is composed of 1 fixed base, 1 MP, and 4 newly designed cable and pulley differentials. Because of
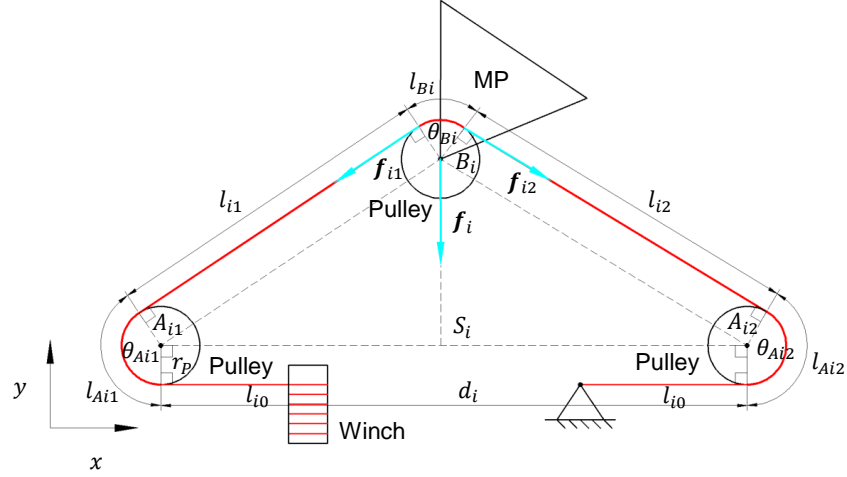
Fig. 2. Schematic of the i-th cable and pulley differential with extra pulley on the CPR.

adopting the novel cable and pulley differential in Fig. **??**, the radius of the pulley will not affect the kinematics and statics of the proposed robot. In Fig. **??**, the red lines represent the cables that actuated by the novel cable and pulley differentials and the blue lines represent the auxiliary vectors used to describe the robot. The fixed frame attached on the base is named as $\mathcal{K}_A$ and the moving frame attached on the MP is named as $\mathcal{K}_B$. For the i-th cable and pulley differential ($i = 1 \cdots 4$), two pulleys are fixed on the base at points A_{i1} and A_{i2} and their position vectors in frame $\mathcal{K}_A$ are denoted as $\boldsymbol{a}_{i1}$ and $\boldsymbol{a}_{i2}$, respectively. Another pulley is attached on the MP at point B_i and its position vector in frame $\mathcal{K}_B$ is named as $\boldsymbol{b}_i$. The cable length between points B_i and A_{i1} is l_{i1} and its direction is denoted as the unit length vector $\boldsymbol{u}_{i1}$. Similarly the cable length between points B_i and A_{i2} is l_{i2} and its direction is denoted as the unit length vector $\boldsymbol{u}_{i2}$. The position vector of the MP in frame $\mathcal{K}_A$ is defined as $\boldsymbol{p}$ and the orientation of the MP with respect to frame $\mathcal{K}_A$ is described by the rotation matrix $\boldsymbol{R}$ and the angle ϕ. Thus the pose of the MP in the fixed frame $\mathcal{K}_A$ is defined as $\boldsymbol{y} = [\boldsymbol{p}^T \ \phi]^T$.

Based on the above definitions, the vector loops in Fig. **??** can be formulated as

$$l_{i1}\boldsymbol{u}_{i1} = \boldsymbol{a}_{i1} - \boldsymbol{p} - \boldsymbol{R}\boldsymbol{b}_i, \tag{17}$$

$$l_{i2}\boldsymbol{u}_{i2} = \boldsymbol{a}_{i2} - \boldsymbol{p} - \boldsymbol{R}\boldsymbol{b}_i. \tag{18}$$

According to (**??**), the effective cable length for the i-th cable and pulley differential is calculated as

$$\begin{aligned} l_i &= l_{i1} + l_{i2} \\ &= ||\boldsymbol{a}_{i1} - \boldsymbol{p} - \boldsymbol{R}\boldsymbol{b}_i||_2 + ||\boldsymbol{a}_{i2} - \boldsymbol{p} - \boldsymbol{R}\boldsymbol{b}_i||_2. \end{aligned} \tag{19}$$

Taking the derivative of (**??**) and we have

$$\dot{l}_i = -[\boldsymbol{u}_{i1}^T + \boldsymbol{u}_{i2}^T \quad \det([\boldsymbol{R}\boldsymbol{b}_i \ \boldsymbol{u}_{i1}]) + \det([\boldsymbol{R}\boldsymbol{b}_i \ \boldsymbol{u}_{i2}])]\dot{\boldsymbol{y}}, \tag{20}$$

where $\dot{\boldsymbol{y}} = [\dot{\boldsymbol{p}}^T \ \dot{\phi}]^T$ represents the twist of the MP. According to (**??**), the Jacobian matrix of the proposed CPR is defined as

$$\boldsymbol{J} = \begin{bmatrix} \boldsymbol{u}_{11}^T + \boldsymbol{u}_{12}^T & \det([\boldsymbol{R}\boldsymbol{b}_1 \ \boldsymbol{u}_{11}]) + \det([\boldsymbol{R}\boldsymbol{b}_1 \ \boldsymbol{u}_{12}]) \\ & \vdots \\ \boldsymbol{u}_{41}^T + \boldsymbol{u}_{42}^T & \det([\boldsymbol{R}\boldsymbol{b}_4 \ \boldsymbol{u}_{41}]) + \det([\boldsymbol{R}\boldsymbol{b}_4 \ \boldsymbol{u}_{42}]) \end{bmatrix}. \tag{21}$$
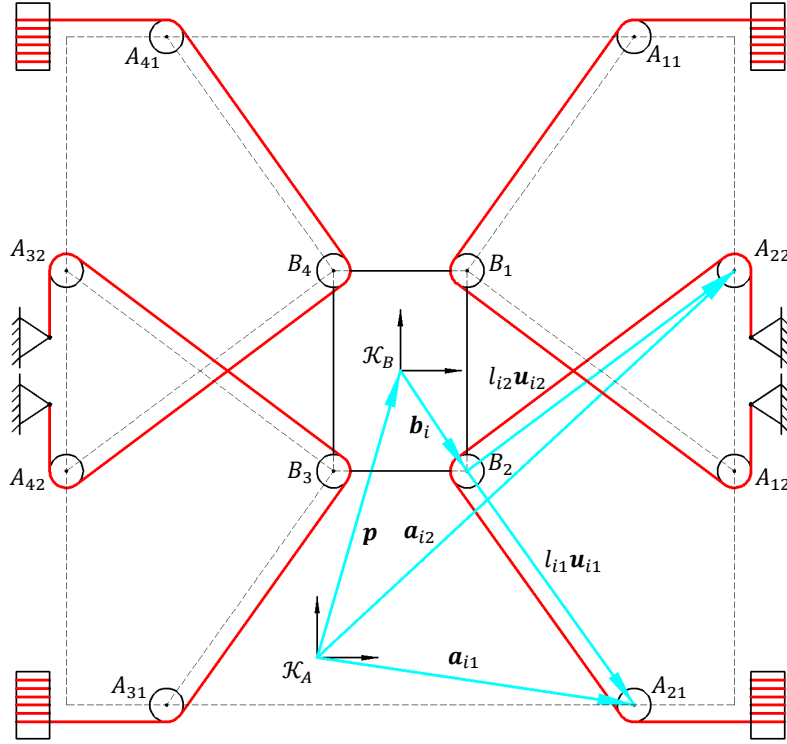
Fig. 3. Schematic of the planar differentially driven CPR.

Hence we have the following relation which maps the twist of the MP to the velocity of cables

$$\dot{\boldsymbol{l}} = -\boldsymbol{J}\dot{\boldsymbol{y}}, \tag{22}$$

where $\boldsymbol{\dot{l}} = [\dot{l}_1 \ \cdots \ \dot{l}_4]^T$ represents the vector of cable velocities.

3.2. Statics Analysis
Assuming the cable tension for the i-th cable and pulley differential is t_i. According to (**??**), the resultant wrench applied by the i-th differential on the MP is

$$\boldsymbol{w}_i = t_i \begin{bmatrix} \boldsymbol{u}_{i1} + \boldsymbol{u}_{i2} \\ \det([\boldsymbol{R}\boldsymbol{b}_i \ \boldsymbol{u}_{i1}]) + \det([\boldsymbol{R}\boldsymbol{b}_i \ \boldsymbol{u}_{i2}]) \end{bmatrix}. \tag{23}$$

Thus we have the following relation which maps the cable forces to the wrench applied on the MP

$$\boldsymbol{w} = \boldsymbol{J}^T\boldsymbol{t}, \tag{24}$$

where $\boldsymbol{w} = \boldsymbol{w}_1 + \cdots + \boldsymbol{w}_4$ represents the resultant wrench applied by all cables on the MP and $\boldsymbol{t} = [t_1 \ \cdots \ t_4]^T$ denotes the vector of cable tensions.

3.3. Stiffness Analysis
One of the main defects of the CPRs is the low stiffness caused by the flexibility of cables. Hence it's of great importance to ensure high stiffness when designing CPRs. Based on

(**??**) and (**??**), the stiffness matrix of the proposed CPR can be derived as

$$\boldsymbol{K} = -\frac{d\boldsymbol{w}}{d\boldsymbol{y}}$$

$$= \boldsymbol{J}^T \boldsymbol{\Omega} \boldsymbol{J} - \frac{d\boldsymbol{J}^T}{d\boldsymbol{y}} \boldsymbol{t}, \tag{25}$$

where $\boldsymbol{\Omega} = diag(\frac{k_e}{l_1} \ \cdots \ \frac{k_e}{l_4})$ and k_e represents the stiffness per unit length of cables used in the proposed CPR. The component $\boldsymbol{J}^T \boldsymbol{\Omega} \boldsymbol{J}$ is called the elastic stiffness matrix which depends on the stiffness of cables. The component $\frac{d\boldsymbol{J}^T}{d\boldsymbol{y}} \boldsymbol{t}$ is called the active stiffness matrix which depends both on pose of the robot and cable tensions. Since the elastic stiffness has generally a much higher effect than the active stiffness on the overall stiffness of the robot, only the elastic stiffness matrix $\boldsymbol{J}^T \boldsymbol{\Omega} \boldsymbol{J}$ is considered in later sections.

4. Performance Indices for Optimization and Comparison
To evaluate the performance of the proposed differentially driven CPR, several performance indices commonly used for CPRs are introduced in this section. Some of the introduced indices will be selected as objective functions for the multi-objective optimal design of the proposed robot. The other indices will be used to verify the performance of the proposed robot comparing with a fully actuated CPR.

4.1. Total Orientation Wrench Closure Workspace
Due to the unilateral property of cables, the workspaces of CPRs are mainly constrained by the cable force conditions. The wrench closure workspace (WCW) for a CPR is defined as the set of poses which there exists a solution satisfying $\boldsymbol{w} = \boldsymbol{J}^T \boldsymbol{t}$ and $\boldsymbol{t} \geq 0$ for any applied wrench $\boldsymbol{w} \in \mathbb{R}^3$. A pose belongs to the WCW means that through keeping cables in tension, any wrench can be applied on the MP. The WCW depends only on the geometry of CPRs. For a planar 4-cable-driven CPR, a pose can be easily tested whether it belongs to the WCW by checking if $\boldsymbol{t}_0$ satisfies $\boldsymbol{t}_0 > 0$ or $\boldsymbol{t}_0 < 0$ with

$$\boldsymbol{t}_0 = \begin{bmatrix} \det([\boldsymbol{J}_2^T \ \boldsymbol{J}_3^T \ \boldsymbol{J}_4^T]) \\ -\det([\boldsymbol{J}_1^T \ \boldsymbol{J}_3^T \ \boldsymbol{J}_4^T]) \\ \det([\boldsymbol{J}_1^T \ \boldsymbol{J}_2^T \ \boldsymbol{J}_4^T]) \\ -\det([\boldsymbol{J}_1^T \ \boldsymbol{J}_2^T \ \boldsymbol{J}_3^T]) \end{bmatrix}, \tag{26}$$

where $\boldsymbol{J}_i^T$ denotes the i-th column of the wrench matrix $\boldsymbol{J}^T$.[?] The total orientation workspace (TOW) is the set of MP positions $\boldsymbol{p}$ which for a given set $\mathcal{R}_0$, all the orientations $\boldsymbol{R} \in \mathcal{R}_0$ are in the workspace. The TOW can be obtained by intersecting all the constant orientation workspaces which the orientations are in the set $\mathcal{R}_0$. Hence the total orientation wrench closure workspace (TOWCW) of the planar 4-cable-driven CPR is defined as the set of MP positions $\boldsymbol{p}$ which for any orientation $\boldsymbol{R} \in \mathcal{R}_0$, $\boldsymbol{t}_0$ satisfies $\boldsymbol{t}_0 > 0$ or $\boldsymbol{t}_0 < 0$. The TOWCW can be determined using the numerical boundary method in ref. [**?**]. This method is based on the discrete investigation of different orientations at one point and using the line search method to iteratively calculate the boundary of the workspace. To describe the size of the workspace, the area of the TOWCW approximated by the numerical boundary method is denoted as a_{TOWCW}.

4.2. Normalized Jacobian Matrix
Many performance indices in robotics are derived using the Jacobian matrix $\boldsymbol{J}$ or its transpose $\boldsymbol{J}^T$. Because the proposed planar CPR has 3 DOFs, which include 2 translational DOFs and 1 rotational DOF, different units appear in the translational part and the rotational part of the Jacobian matrix $\boldsymbol{J}$. To alleviate this problem, the

normalized Jacobian matrix $\hat{\boldsymbol{J}}$ is defined as

$$\hat{\boldsymbol{J}} = \boldsymbol{J}\,diag(1\ 1\ \frac{m}{\sum_{i=1}^{m}||\boldsymbol{b}_i||_2}), \tag{27}$$

where $m = 4$ is the number of attachment points on the MP.

4.3. Kinematic Isotropy Index
The kinematic isotropy index (KII) is defined as

$$\mathrm{KII} = \frac{\sigma_{\min}}{\sigma_{\max}}, \tag{28}$$

where $\sigma_{\min}$ and $\sigma_{\max}$ are the minimum singular value and the maximum singular value of the normalized Jacobian matrix $\hat{\boldsymbol{J}}$ respectively. The KII is also called the dexterity index, which represents the robot's local kinematic behaviour. The Jacobian matrix is well-conditioned when the KII approaches 1. To measure the kinematic performance over the workspace, the global kinematic isotropic index (GKII) is defined as

$$\mathrm{GKII} = \frac{1}{N_w}\sum_{i=1}^{N_w}\mathrm{KII}_i, \tag{29}$$

where N_w represents the number of discrete poses which lie in the TOWCW.

4.4. Manipulability Index
The manipulability index is defined as

$$\mathrm{MI} = \prod_{i=1}^{n}\sigma_i, \tag{30}$$

where σ_i denote the singular values of the normalized Jacobian matrix $\hat{\boldsymbol{J}}$ and $n = 3$ is the number of DOFs. The MI represents locally the efficiency of the twist and wrench transmission of the robot. Similar with the GKII, the global manipulability index (GMI) is defined as

$$\mathrm{GMI} = \frac{1}{N_w}\sum_{i=1}^{N_w}\mathrm{MI}_i. \tag{31}$$

4.5. Stiffness Isotropy Index
Using the normalized Jacobian matrix $\hat{\boldsymbol{J}}$, the normalized elastic stiffness matrix of the robot is defined as

$$\hat{\boldsymbol{K}}_e = \hat{\boldsymbol{J}}^T\boldsymbol{\Omega}\hat{\boldsymbol{J}}. \tag{32}$$

The stiffness isotropy index (SII) is defined as

$$\mathrm{SII} = \frac{\lambda_{\min}}{\lambda_{\max}}, \tag{33}$$

where $\lambda_{\min}$ and $\lambda_{\max}$ are the minimum eigenvalue and the maximum eigenvalue of the normalized elastic stiffness matrix $\hat{\boldsymbol{K}}_e$, respectively. The SII represents the local stiffness distribution along different DOFs. In order to measure the stiffness distribution over the

workspace, the global stiffness isotropy index (GSII) is defined as

$$\text{GSII} = \frac{1}{N_w} \sum_{i=1}^{N_w} \text{SII}_i. \tag{34}$$

4.6. Stiffness Magnitude Index
The stiffness magnitude index (SMI) is defined as

$$\text{SMI} = \frac{\lambda_{\min}^2 \lambda_{\max}^2}{\lambda_{\min}^2 + \lambda_{\max}^2}. \tag{35}$$

The SMI captures the local stiffness magnitude of the robot and it has high value when $\lambda_{\min}$ and $\lambda_{\max}$ are equal and large. The global stiffness magnitude index (GSMI) is defined as

$$\text{GSMI} = \frac{1}{N_w} \sum_{i=1}^{N_w} \text{SMI}_i. \tag{36}$$

4.7. Tension Factor
The tension factor (TF) of cable parallel robots is proposed in ref. [**?**] to evaluate the tension distribution among cables. The isotropic vector which represents the uniform distribution of cable tension is projected onto the null space of the wrench matrix $\boldsymbol{J}^T$ and the obtained homogeneous solution is used to calculate the TF. The definition of TF is as follows

$$\text{TF} = \frac{\min(\boldsymbol{f}_N)}{\max(\boldsymbol{f}_N)}, \tag{37}$$

with

$$\begin{aligned}
\boldsymbol{f}_N &= \text{proj}_{\text{null}(\boldsymbol{J}^T)}(\boldsymbol{t}_I) \\
&= (\boldsymbol{I} - \boldsymbol{J}^{+T} \boldsymbol{J}^T) \boldsymbol{t}_I,
\end{aligned} \tag{38}$$

where $\boldsymbol{J}^{+T}$ is the Moore–Penrose inverse of the wrench matrix $\boldsymbol{J}^T$ and $\boldsymbol{t}_I = [1 \ \cdots \ 1]^T$ is the isotropic vector. The robot has a uniform tension distribution among the cables when the TF approaches 1. The global tension factor (GTF) is defined as

$$\text{GTF} = \frac{1}{N_w} \sum_{i=1}^{N_w} \text{TF}_i. \tag{39}$$

5. Multi-Objective Optimal Design of the Differentially Driven CPR
In order to make the proposed robot valuable in practical tasks, it's necessary to optimize the structural parameters of the proposed robot to exert its best performance. In this section, a multi-objective optimization approach is proposed to determine the structural parameters of the proposed differentially driven CPR.

5.1. Design Parameters
The optimal design for a CPR is to determine the positions of the attachment points on the base and the MP. To reduce the design parameters of the proposed robot, the attachment points on the base are all assumed to locate on a circle with the radius r_A, and the attachment points on the MP are all assumed to locate on a circle with the radius r_B. To have a symmetric workspace, the geometry of the base and the MP is designed to be symmetrical along the x and y axes of the plane. Defining the angle between the

x axis of the fixed frame $\mathcal{K}_A$ and vectors $\boldsymbol{a}_{11}$ and $\boldsymbol{a}_{12}$ as ψ_{A1} and ψ_{A2} respectively, then the positions of the attachment points on the base expressed in frame $\mathcal{K}_A$ are as follows

$$\boldsymbol{a}_{11} = r_A \left[\cos \psi_{A1} \ \sin \psi_{A1}\right] \qquad \boldsymbol{a}_{12} = r_A \left[\cos \psi_{A2} \ \sin \psi_{A2}\right] \tag{40}$$

$$\boldsymbol{a}_{21} = r_A \left[-\cos \psi_{A1} \ \sin \psi_{A1}\right] \qquad \boldsymbol{a}_{22} = r_A \left[-\cos \psi_{A2} \ \sin \psi_{A2}\right] \tag{41}$$

$$\boldsymbol{a}_{31} = r_A \left[-\cos \psi_{A1} \ -\sin \psi_{A1}\right] \qquad \boldsymbol{a}_{32} = r_A \left[-\cos \psi_{A2} \ -\sin \psi_{A2}\right] \tag{42}$$

$$\boldsymbol{a}_{41} = r_A \left[\cos \psi_{A1} \ -\sin \psi_{A1}\right] \qquad \boldsymbol{a}_{42} = r_A \left[\cos \psi_{A2} \ -\sin \psi_{A2}\right]. \tag{43}$$

Defining the angle between the x axis of the moving frame $\mathcal{K}_B$ and vectors $\boldsymbol{b}_1$ as ψ_B, the positions of the attachment points on the MP expressed in frame $\mathcal{K}_B$ are

$$\boldsymbol{b}_1 = r_B \left[\cos \psi_B \ \sin \psi_B\right] \qquad \boldsymbol{b}_2 = r_B \left[-\cos \psi_B \ \sin \psi_B\right] \tag{44}$$

$$\boldsymbol{b}_3 = r_B \left[-\cos \psi_B \ -\sin \psi_B\right] \qquad \boldsymbol{b}_4 = r_B \left[\cos \psi_B \ -\sin \psi_B\right]. \tag{45}$$

In this work, the three angles ψ_{A1}, ψ_{A2} and ψ_B are chosen as the design parameters. The limitations of these design parameters are set to

$$-\frac{\pi}{2} < \psi_{A1} < \frac{\pi}{2}, \quad -\frac{\pi}{2} < \psi_{A2} < \frac{\pi}{2}, \quad 0 < \psi_B < \frac{\pi}{2}. \tag{46}$$

The other parameters used in optimization are set as follows. The radius of the fixed base and the radius of the MP are set to $r_A = 1$ m and $r_B = 0.1$ m respectively. The cable stiffness constant k_e is set to $k_e = 20000$ N/m. To define the TOWCW, the orientation set $\mathcal{R}_0$ is defined by the angle region $\phi \in [-\frac{\pi}{6}, \frac{\pi}{6}]$.

5.2. Objective Functions

One of the most important properties of CPRs is the large workspace which makes the CPRs capable of performing various tasks. While the main drawbacks of CPRs are high flexibility and relative low positioning accuracy. So the objective of the optimal design is to obtain a CPR with large workspace and high stiffness magnitude. The a_{TOWCW} and the GSMI are selected as objective functions for the multi-objective optimal design. According to the definitions in Section ??, a high a_{TOWCW} means that the robot can achieve static equilibrium in a large area with any applied wrench, and a high GSMI means that the robot has large stiffness magnitude over the workspace. Both of the two indices are taken negative values in order to shape the problem into a standard form. The limitation on cable tension is ignored here because the size of WCW is considered. The interference between cables or between cable and the MP is not considered because it's not a critical issue for planar robots.

Thus the multi-objective optimal design of the proposed differentially driven CPR is described as

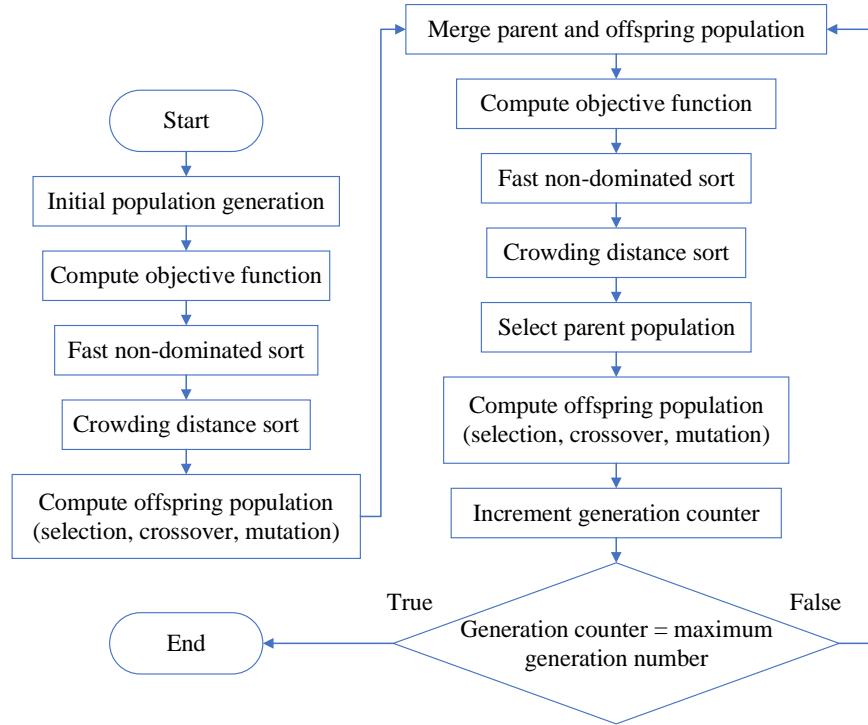$$\min \begin{cases} g_1 = -a_{\text{TOWCW}} \\ g_2 = -\text{GSMI} \end{cases} \tag{47}$$

subject to

$$\boldsymbol{x} = [\psi_{A1} \ \psi_{A2} \ \psi_B]^T, \tag{48}$$

$$[-\frac{\pi}{2} \ -\frac{\pi}{2} \ 0]^T < \boldsymbol{x} < [\frac{\pi}{2} \ \frac{\pi}{2} \ \frac{\pi}{2}]^T. \tag{49}$$

5.3. Solving Algorithm

The multi-objective optimal design for the proposed differentially driven CPR is solved by the non-dominated sorting genetic algorithm II (NSGA-II). The NSGA-II is an evolutionary elitist algorithm inspired by the natural evolutionary process which is

o w chart.p df

Fig. 4. Flow-chart of the main procedure of the NSGA-II.

able to handle highly nonlinear optimization problems. Benefiting from the fast non-dominated sorting procedure, the elitist strategy, the parameterless approach, and the efficient constraint-handling method, the NSGA-II has lower computational complexity, a better spread of solutions, and better convergence in the non-dominated front compared with other multi-objective evolutionary algorithms (MOEAs). The main procedure of the NSGA-II is shown in Fig. **??**. It starts from a randomly generated initial population, goes through a series of sorting, selection, crossover, and mutation, and constantly updates the population until the maximum generation number is reached.

The NSGA-II is implemented in MATLAB based on ref. [**?**]. In our implementation, the population size is set to 200, the crossover probability is set as 0.9, the mutation probability is set to 0.5, the maximum generation number is set to 100, and the mutation strength is set to 0.05.

5.4. Results Selection

Fig. **??** shows the optimization process using the NSGA-II and the obtained Pareto front. The blue dots represent the individuals of the population in each generation during the optimization process. The set of black circles represents the Pareto front obtained in the last generation. The Pareto front is the solution set of Pareto-optimal solutions, which mean that no objective function can be improved without making at least one other objective function worse or still. In Fig. **??**, the randomly generated initial population undergoes continuous evolution and is evenly distributed to the Pareto front in the end.

In order to select an optimal solution from the Pareto front, the GKI I is calculated for all the Pareto-optimal solutions. Since the solutions in the Pareto front are optimal for workspace and stiffness magnitude, we also wish the robot to have better kinematic behaviour among the workspace. A higher GKI I means that the robot could move more isotropically over the workspace. Thus the solution with the maximal GKI I in the Pareto front is selected as the final solution. The design parameters corresponding to the final
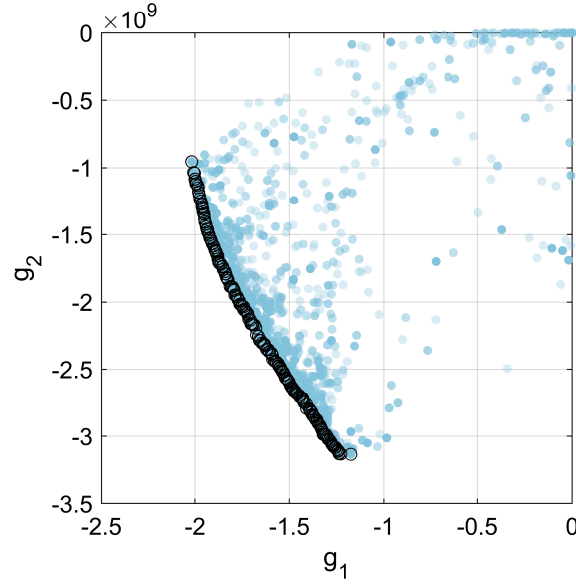
Fig. 5. The optimization process using the NSGA-II for the differentially driven CPR.

optimal solution are

$$\psi_{A1} = -1.3085 \text{ rad}, \tag{50}$$

$$\psi_{A2} = -0.1026 \text{ rad}, \tag{51}$$

$$\psi_B = 0.9737 \text{ rad}. \tag{52}$$

The corresponding performance indices of the obtained robot are

$$a_{\text{TOWCW}} = 1.9281 \text{ m}^2, \tag{53}$$

$$\text{GSMI} = 1.5049 \times 10^9, \tag{54}$$

$$\text{GKII} = 0.7475. \tag{55}$$

Fig. **??** shows the geometry of the finally obtained differentially driven CPR. The obtained robot is plotted with pose $y = [0\ 0\ 0]^T$. The red lines represent the actuated cables and the black lines represent the base and MP. The boundary of the TOWCW for the obtained robot is shown in Fig. **??**.

6. Comparison with the Fully Actuated CPR

To show the effects of the cable differentials on the design of CPRs, our proposed differentially driven CPR is evaluated by comparing the performance indices with a 3-DOF planar fully actuated CPR. For the fully actuated CPR, the main difference compared with the proposed CPR is that the attachment points A_{i2} in Fig. **??** are deleted. Four cables exist from the winches go through points A_{i1} and are directly attached on the MP at points B_i. Hence the design parameters for the fully actuated CPR are only ψ_{A1} and ψ_B. The fully actuated CPR used for comparison is designed through the same procedure in Fig. **??**. The multi-objective optimization process for the fully actuated CPR is shown in Fig. **??**. The blue dots represent the individuals of the population in each generation during the optimization process. The set of black circles represents the Pareto front obtained in the last generation. The optimal solution is selected from the Pareto front based on GKII. The optimized fully actuated CPR is shown in Fig. **??**
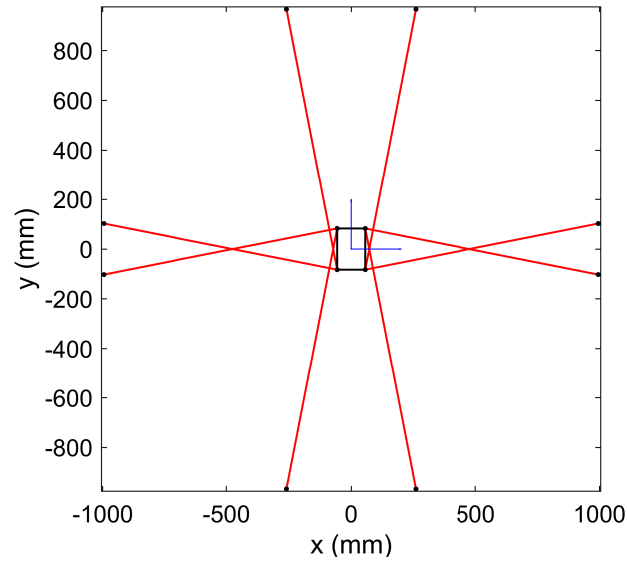
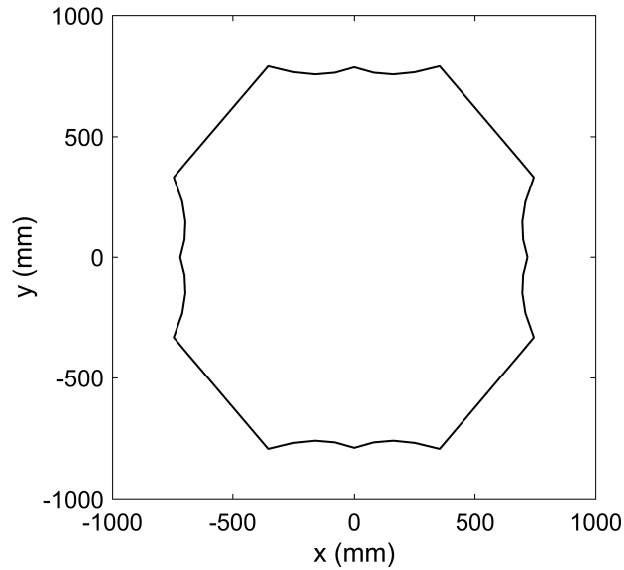Fig. 6. The obtained differentially driven CPR from multi-objective optimal design.

Fig. 7. The boundary of the TOWCW of the obtained differentially driven CPR.

with pose $y = [0\ 0\ 0]^T$. The red lines represent the actuated cables and the black lines represent the base and MP. The TOWCW of the obtained fully actuated CPR is shown in Fig. ??. The corresponding design parameters for the obtained fully actuated CPR are

$$\psi_{A1} = -0.6959 \text{ rad},\tag{56}$$

$$\psi_B = 1.0466 \text{ rad}.\tag{57}$$

Fig. ?? and Fig. ?? demonstrate the effectiveness of the optimization algorithm. The Pareto front obtained in Fig. ?? is much wider than the Pareto front in Fig. ??, since the design parameters of differentially driven CPR have a higher dimension than that
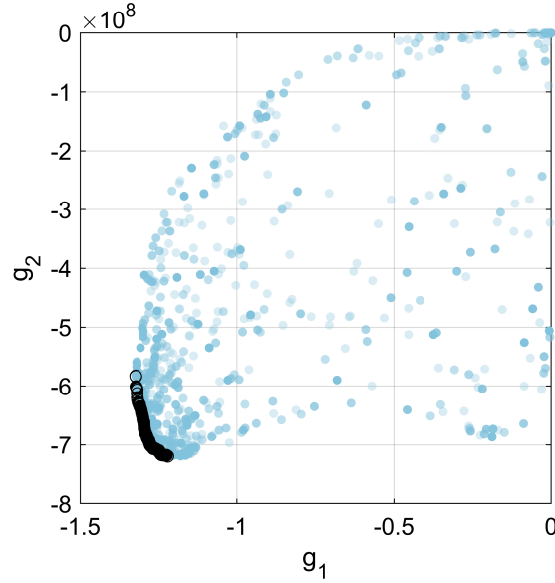
Fig. 8. The optimization process using the NSGA-II for the fully actuated CPR.

of fully actuated CPR, which gives differentially driven CPR the ability to achieve better performance. Fig. **??** and Fig. **??** show that the optimal structures for both the differentially driven and fully actuated CPRs are with the crossed-cable layout, since the crossed-cable layout could improve the stiffness and ability to resist external wrench of CPRs. By comparing Fig. **??** and Fig. **??**, it can be seen that the differentially driven CPR has a larger and more circular TOWCW compared with the fully actuated CPR. The comparison of the performance indices of the differentially driven and the fully actuated CPRs are shown in Table **??**. From the comparison results, it can be seen that the differentially driven CPR has better performances than the fully actuated CPR in most of these aspects except for the GTF. The results of a_{TOWCW} indicate that the proposed differentially driven CPR could work in a larger workspace compared with the fully actuated CPR. The results of GKII and GMI indicate that the proposed CPR has better kinematic and static performance over the workspace compared with the fully actuated CPR. The results of GSII and GSMI indicate that the proposed CPR has better stiffness distribution and stiffness magnitude over the workspace compared with the fully actuated CPR. While the results of GTF indicate that the fully actuated CPR has a more uniform tension distribution among cables over the workspace compared with the proposed CPR.

The improvement of performances can be explained by three reasons. Firstly, using the cable and pulley differentials cause the change of positions of the virtual attachment points on the base, so cables can apply wrenches on the MP from more directions. Secondly, the cable differentials make the resultant forces of cables have a much larger magnitude than the forces exerted by single cables. Finally, more cables that connect the base and the MP with the same number of actuators make the performance indices vary more uniformly over the workspace. While the decrease of the GTF is due to the small wrapping angles around the pulleys on the MP close to the border of the workspace which causes inefficient force transmission of the cable and pulley differentials.

7. Conclusions

In this work, a novel planar CPR actuated by four cables and pulley differentials is designed and analyzed. The new cable and pulley differential with an extra pulley on the base eliminates the modeling inaccuracies due to the pulley radius and obviates the
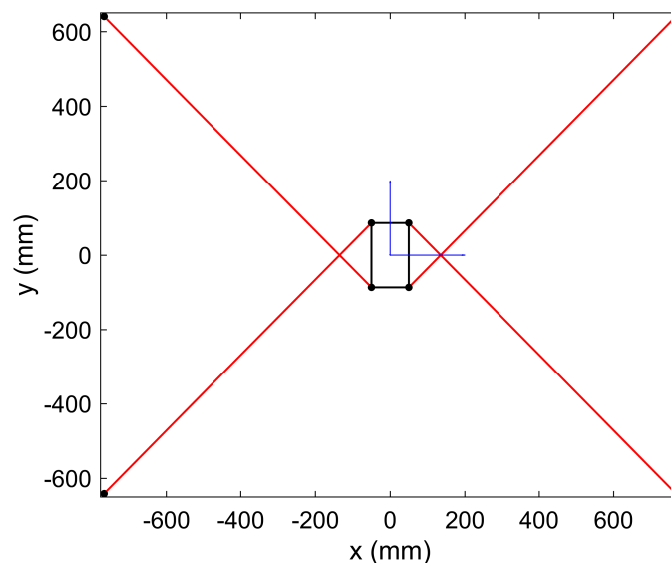
Fig. 9. The obtained fully actuated CPR from multi-objective optimal design.
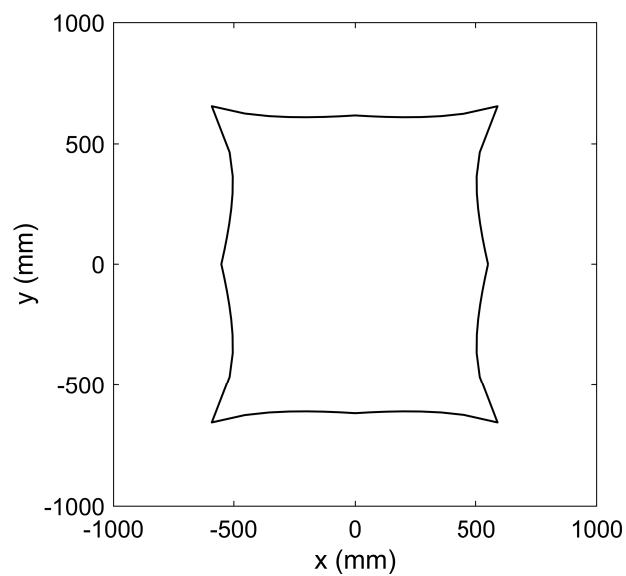

Fig. 10. The boundary of the TOWCW of the obtained fully actuated CPR.

Table I . Comparison of the differentially driven and the fully actuated CPRs.

Performance indices	Differentially driven	Fully actuated
a_{TOWCW}	1.9281 m^2	1.3029 m^2
GKII	0.7475	0.6999
GMI	16.0938	3.4618
GSII	0.5100	0.3841
GSMI	1.5049×10^9	6.5364×10^8
GTF	0.4035	0.4952

need of solving the complex model which considers the pulley kinematics. The geometry of the proposed CPR is optimized for the largest TOWCW and the highest GSMI. The proposed differentially driven CPR is evaluated by comparing its performance with a fully actuated CPR driven by the same number of actuators. The comparison results show that the proposed differentially driven CPR has better performance in most of the aspects. The future work is to develop this approach to design spatial differentially driven CPRs and build a real prototype.

Acknowledgements

References

1. J. Begey, L. Cuvillon, M. Lesellier, M. Gouttefarde, and J. Gangloff, "Dynamic control of parallel robots driven by flexible cables and actuated by position-controlled winches," *IEEE Trans. Rob.* **35**(1), 286–293 (2018).
2. C. Gosselin, "Cable-driven parallel mechanisms: state of the art and perspectives," *Mechanical Engineering Reviews* **1**(1), DSM0004–DSM0004 (2014).
3. D. Zanotto, G. Rosati, S. Minto, and A. Rossi, "Sophia-3: A semiadaptive cable-driven rehabilitation device with a tilting working plane," *IEEE Trans. Rob.* **30**(4), 974–979 (2014).
4. G. Mottola, C. Gosselin, and M. Carricato, "Dynamically feasible motions of a class of purely-translational cable-suspended parallel robots," *Mech. Mach. Theory* **132**, 193–206 (2019).
5. G. Abbasnejad, J. Eden, and D. Lau, "Generalized ray-based lattice generation and graph representation of wrench-closure workspace for arbitrary cable-driven robots," *IEEE Trans. Rob.* **35**(1), 147–161 (2018).
6. H. Khakpour, L. Birglen, and S. A. Tahan, "Synthesis of differentially driven planar cable parallel manipulators," *IEEE Trans. Rob.* **30**(3), 619–630 (2014).
7. H. Khakpour and L. Birglen, "Workspace augmentation of spatial 3-dof cable parallel robots using differential actuation," **In**: *Proceedings of the IEEE/RSJ International Conference on Intelligent Robots and Systems*, Chicago (2014) pp. 3880–3885.
8. H. Khakpour, L. Birglen, and S. A. Tahan, "Analysis and optimization of a new differentially driven cable parallel robot," *ASME J. Mech. Rob.* **7**(3), 034503-034503 (2015).
9. L. Birglen and M. Gouttefarde, "Stiffness of planar 2-dof 3-differential cable-driven parallel robots," **In**: *Proceedings of the International Conference on Cable-Driven Parallel Robots*, (2019) pp. 61–71.
10. H. Liu, C. Gosselin, and T. Laliberte, "Conceptual design and static analysis of novel planar spring-loaded cable-loop-driven parallel mechanisms," *ASME J. Mech. Rob.* **4**(2), 021001–021001 (2012).
11. M. Filipovic, A. Djuric, and L. Kevac, "The rigid s-type cable-suspended parallel robot design, modelling and analysis," *Robotica* **34**(9), 1948–1960 (2016).
12. M. Gouttefarde, J. F. Collard, N.s Riehl, and C. Baradat, "Geometry selection of a redundantly actuated cable-suspended parallel robot," *IEEE Trans. Rob.* **31**(2), 501–510 (2015).
13. G. Boschetti and A. Trevisani, "Cable robot performance evaluation by wrench exertion capability," *Robotics* **7**(2), 15–15 (2018).
14. Z. Zhang, Z. Shao, F. Peng, H. Li, and L. Wang, "Workspace analysis and optimal design of a translational cable-driven parallel robot with passive springs," *ASME J. Mech. Rob.* **12**(5), 051005–051005 (2020).
15. I. B. Hamida, M. A. Laribi, A. Mlika, L. Romdhane, S. Zeghloul, and G. Carbone, "Multi-objective optimal design of a cable driven parallel robot for rehabilitation tasks," *Mech. Mach. Theory* **156**, 104141–104141 (2021).
16. A. Gonzalez-Rodriguez, F. J. Castillo-Garcia, E. Ottaviano, P. Rea, and A. G. Gonzalez-Rodriguez, "On the effects of the design of cable-driven robots on kinematics and dynamics models accuracy," *Mechatronics* **43**, 18–27 (2017).
17. X. Jin, J. Jung, J. Piao, E. Choi, J. O. Park, and C. S. Kim, "Solving the pulley inclusion problem for a cable-driven parallel robotic system: Extended kinematics and twin-pulley mechanism," *J. Mech. Sci. Technol.* **32**(6), 2829–2838 (2018).
18. H. Lamine, L. Romdhane, H. Saafi, and S. Bennour, "Design-to-workspace synthesis of a cable robot used in legs training machine," *Robotica* **38**(9), 1703–1714 (2020).
19. M. Gouttefarde and C. Gosselin, "Analysis of the wrench-closure workspace of planar parallel cable-driven mechanisms," *IEEE Trans. Rob.* **22**(3), 434–445 (2006).
20. A. Pott, "Efficient computation of the workspace boundary, its properties and derivatives for cable-driven parallel robots," **In**: *Proceedings of the International Workshop on Computational Kinematics*, Futuroscope-Poitiers (2017) pp. 190–197.

21. C. B. Pham, S. H. Yeo, G. Yang, and I. M. Chen, "Workspace analysis of fully restrained cable-driven manipulators," *Rob. Auton. Syst.* **57**(9), 901–912 (2009).
22. K. Deb, A. Pratap, S. Agarwal, and T. Meyarivan, "A fast and elitist multiobjective genetic algorithm: Nsga-ii," *IEEE Trans. Evol. Comput.* **6**(2), 182–197 (2002).